JGR Atmospheres

RESEARCH ARTICLE
10.1029/2019JD031828

Evidence for Horizontal Blocking and Reflection of a Small-Scale Gravity Wave in the Mesosphere

N. R. Criddle[1], P.-D. Pautet[1], T. Yuan[1,2], C. Heale[3], J. Snively[3], Y. Zhao[1], and M. J. Taylor[1,2]

[1]Center for Atmospheric and Space Sciences, Utah State University, Logan, UT, USA, [2]Physics Department, Utah State University, Logan, UT, USA, [3]Center for Space and Atmospheric Research and Department of Physical Sciences, Embry-Riddle Aeronautical University, Daytona Beach, FL, USA

Key Points:
- We observe blocking and reflection of a small-scale gravity wave
- The wave blocking event occurred when the wave was experiencing strong and increasing headwind
- The wave was propagating in an upper mesosphere temperature inversion layer formed within the OH layer

Correspondence to:
T. Yuan,
titus.yuan@usu.edu

Citation:
Criddle, N. R., Pautet, P.-D., Yuan, T., Heale, C., Snively, J., Zhao, Y., & Taylor, M. J. (2020). Evidence for horizontal blocking and reflection of a small-scale gravity wave in the mesosphere. *Journal of Geophysical Research: Atmospheres*, *124*, e2019JD031828. https://doi.org/10.1029/2019JD031828

Received 13 OCT 2019
Accepted 15 APR 2020
Accepted article online 19 APR 2020

Author Contributions:
Conceptualization: N. R. Criddle
Data curation: N. R. Criddle, P.-D. Pautet
Formal analysis: N. R. Criddle
Funding acquisition: T. Yuan
Investigation: N. R. Criddle
Methodology: N. R. Criddle
Project administration: T. Yuan
Resources: P.-D. Pautet, Y. Zhao
Software: N. R. Criddle
Supervision: M. J. Taylor
Validation: P.-D. Pautet
Writing – review & editing: P.-D. Pautet

Abstract The variations of the horizontal phase velocity of an internal gravity wave, generated by wave "blocking" or "reflection" due to an inhomogeneous wind field, have been predicted theoretically and numerically investigated but had yet to be captured experimentally. In this paper, through a collaborative observation campaign using a sodium (Na) Temperature/Wind lidar and a collocated Advanced Mesospheric Temperature Mapper (AMTM) at Utah State University (USU), we report the first potential evidence of such a unique gravity wave process. The study shows that a small-scale wave, captured by the AMTM, with initial observed horizontal phase velocity of 37 ± 5 m/s toward the northwest direction, experienced a large and increasing headwind as it was propagating in the AMTM field of view. This resulted in significant deceleration along its initial traveling direction, and it became quasi-stationary before it was "reflected" to the opposite direction at later time. The USU Na lidar measured the horizontal wind and temperature during the event, when the wave was found traveling within a temperature inversion layer and experiencing an increasing headwind relative to the wave. The wind agrees well with the expected value for wave blocking suggested by the wave tracing theory, implying the existence of a large horizontal wind gradient that night near the OH layer altitudes. The study indicates the critical role of horizontal winds and their horizontal gradients in determining propagation in vertical and horizontal directions.

1. Introduction

Gravity wave (GW) activity and its associated dynamical features have important effects in the middle and upper atmosphere, where they contribute to atmospheric circulation, transport and mixing, and thermal structure (Fritts & Alexander, 2003). They carry energy and momentum from the troposphere and the stratosphere to higher altitudes, as they propagate outward and upward into the upper atmosphere and ionosphere. The seasonal change of GW filtering in the middle atmosphere alters the variation of GW dissipation and drag in the mesosphere lower thermosphere (MLT), causing seasonal change of vertical adiabatic flow that leads to counterintuitive cold summer and warm winter in the upper mesosphere (Holton, 1983). Further, observations have shown that GWs are ubiquitous in the atmosphere and highly variable in their characteristics, considerably altering the atmospheric dynamics. In the MLT, significant wave dissipation, breaking, and nonlinear wave interactions occur, making this region one of the most complex and the least understood part of the atmosphere. The experimental and numerical investigations over the past decade have greatly advanced our understanding of GW dynamics in the MLT and into the thermosphere and ionosphere, along with their role in various ion-neutral coupling processes (Fritts & Lund, 2011; Liu & Vadas, 2013). While both orographic and deep convection sources have been well recognized and proven as major sources for the GWs observed in the MLT (Fritts & Alexander, 2003 and the references within), investigations have demonstrated wave dissipation and breaking can generate secondary GWs that becomes significant in the MLT and/or above (Becker & Vadas, 2018; Bossert et al., 2017; Snively & Pasko, 2008; Vadas et al., 2003).

It has been well documented that the horizontal wind plays a critical role in GW propagation, affecting the GW intrinsic frequency, $\omega_i = kc_i = k(c - U_h)$ (k is the horizontal wavenumber of the GW, c and U_h are the GW-observed horizontal phase velocity and mean wind in the direction of GW propagation, respectively), and phase speed, $c_i = c - U_h$, both of which vary with respect to the horizontal wind in the wave propagating direction. In addition, based on ray tracing theory, the change of background wind also modulates the

ground relative frequency (the observed frequency) and the associated ground relative phase speed (the observed phase speed). Theoretical works (e.g., Basovich & Tsimring, 1984) studying the effect of horizontal wind shear or gradients on wave propagation also predict the wave "blocking" phenomenon, when the wave's horizontal group velocity becomes zero against an opposing background wind. Heale and Snively (2015) conducted a comprehensive and detailed numerical simulation work on the small-scale GW variations when it encounters vertically and horizontally inhomogeneous wind field, which can be induced by either a large-scale tidal wave modulation or a medium-scale GW. Depending on the relative direction of the wind compared to the wave propagation and the parameters of the small-scale wave, distinct scenarios can occur, including the "blocking" of the small-scale wave. Such large-scale wavelike features in winds directly impact the GW propagation and the associated energy/momentum transfer in MLT. However, no experimental evidence for such GW evolutions (i.e., observed horizontal GW speed dropping to zero, dramatic increase in wave amplitude, and simultaneous decrease in horizontal wavelength) has ever been reported, leaving this theoretical work unconfirmed. One challenge of such an observation lies in the requirement of the instrument cluster, which must have the capabilities of capturing both the temporal and spatial variations in the horizontal wave structure, as well as in the horizontal wind.

The collaborative observations between optical airglow instruments and lidar have been contributing considerably to the understanding of GW dynamics and the associated atmospheric instabilities in the upper atmosphere over the past decades (Bossert et al., 2015; Cai et al., 2014; Fritts et al., 1997; Fritts et al., 2014; Hecht et al., 1997; Li et al., 2005; Lu et al., 2015; Yuan et al., 2014). The MLT above the midlatitude Rocky Mountain Range has proven to be a highly active area for atmospheric GWs, ideal for GW dynamical investigations, because it has contributions from both orographic and deep convective sources. The instrument cluster located in northern Utah comprises the Utah State University (USU) Na Temperature/Wind lidar operated at the USU campus [41.7°N, 111.8°W] and a colocated Advanced Mesospheric Temperature Mapper (AMTM) (Pautet et al., 2014), providing comprehensive measurements on different aspects of the GW activity and variations. These instruments have revealed many new and important features of GW behavior in the MLT over the past a few years: Yuan et al. (2014) found the potential relationship between wave breaking and temperature inversion layer; Fritts et al. (2014) have developed a new method to estimate the momentum flux transported by small-scale GW; Cai et al. (2014) have discussed the small-scale wave breaking induced by the dynamic instability resulting from the superposition of large amplitude tide and a medium-scale GW; Yuan et al. (2016) have discovered the first evidence of dispersion and refraction of a spectrally-broad GW packet, in which the period of a GW packet was found to vary over altitude; Lu et al. (2015) utilized simultaneous observations on both sides of the Rocky Mountain Range (at USU and Boulder, CO) to investigate the horizontal propagation of a 1-hr period GW.

In this paper, as part of this ongoing collaboration, we report a unique GW event that occurred on the night of 11 September 2016 and was captured simultaneously by the USU Na lidar and the AMTM. The AMTM observed that the horizontal phase speed and horizontal wavelength varied considerably during the event. The paper is laid out as follows: A brief description on the instruments involved is in section 2, observations of this event are described in section 3, the discussion of the potential dynamical mechanisms are introduced in section 4, followed by a summary in section 5.

2. Instrumentation

The three-frequency USU Na lidar is a narrowband resonance fluorescence Doppler lidar system operating at the Na D2a line with a 120-MHz full-width at half-maximum (FWHM) laser pulse bandwidth. It obtains high-resolution temperature and horizontal wind profiles, along with Na density profile in the mesopause region (~ 80–105 km), through precisely measuring the Doppler broadening and Doppler shift of the Na fluorescence spectrum in the MLT region in full diurnal cycle (Krueger et al., 2015). Thus, the lidar measurements provide critical atmospheric information throughout a full diurnal cycle of observations of the mesopause region, such as tidal and planetary wave variations of Na density, temperature, and horizontal wind. The binning size of the lidar echo profile is set up as 150 m in the line-of-sight direction, and the photon profile is saved every minute. These profiles are then processed with various temporal and spatial resolutions, depending on the requirements of different scientific topics. In this study, the lidar data is binned with 10-min temporal resolution and using a 2-km FWHM Hanning window sliding in the vertical direction to

achieve good quality results. Here, the data with temperature uncertainty larger than 10 K and wind uncertainty larger than 5 m/s are treated as bad data and are excluded from this study.

The collocated USU AMTM has been designed to measure the mesospheric OH (3, 1) rotational temperatures over an area of ~200 km × 160 km (field of view), centered on the zenith. This instrument uses a fast (*f*/1) 120° field-of-view telecentric lens system designed and built at the Space Dynamics Laboratory, Logan, Utah, and three 4″ narrow band (2.5–3 nm) filters centered on the $P_1(2)$ and $P_1(4)$ lines of the OH (3,1) band, and a nearby background region, mounted in a temperature stabilized filter wheel. The detector is an infrared camera fitted with a 320 × 256 pixel InGaAs sensor, thermoelectrically cooled to −50 °C to limit electronic noise. The exposure time for each filter is typically 10 s, giving precise temperature measurement (1–2 K) every ~30 s. This imager can operate in the presence of aurora and also acquires data under full moon conditions (Pautet et al., 2014). For this study, the AMTM data have temporal resolution of 34 s with temperature measurement uncertainty of 2 K.

3. Observations

Figure 1 shows the full field of view of the AMTM between UT 03:40 (09:40 pm local time) and UT 04:05 (10:05 pm local time) on the night of 11 September 2016, every 5 min. The north edge of the lidar hangar (top of each plot), which also hosts the AMTM, serves as a convenient stationary reference with respect to the traveling of the small-scale GW. The wave was measured to be propagating toward northwest and initially had an observed horizontal phase speed of ~37 ± 5 m/s and horizontal wavelength of ~17 ± 3 km, resulting in an observed period of ~8 ± 2 min, slightly after UT 03:20. The phase speed slowed down to 19 ± 5 m/s at UT 03:35 and kept decreasing. As the figure shows, after UT 03:50, the front of the wave was barely moving along its original direction, appearing to be almost stationary, while the subsequent peaks of the wave kept moving into the field of view behind the leading wave front, causing "compression" of the wave packet. The quasi-stationary wave packet was still visible around UT 04:50 (not shown) but had already started to dissipate into more complex smaller wave structures. The leading front at this time, although much weaker than its initial intensity, still stayed at almost the same location in the field of view. At the end, the horizontal wavelength shortened to ~10 ± 3 km, considerably "compressed." The horizontal scale of this wave packet is clearly demonstrated in Figure 2, which lays the AMTM measurement at UT 04:13, when the wave is fully "blocked," on top of the regional terrain map of northern Utah. The first wave front spanned more than 250 km and never reached the north-pointing Na lidar beam, having little effect on the temperature profile measurements in the lidar North Channel. Looking at the time variations of the wave's horizontal wavelength and phase speed in Figure 3, the decreasing of both horizontal wavelength and phase speed of the small-scale wave is evident. The wave slowed down to its minimum horizontal phase speed of ~6 ± 2 m/s near UT 04:00 when its horizontal wavelength was "compressed" to its minimum of ~9 ± 1 km, almost half of its original wavelength. After UT 04:00, the wavelength increased slightly, while the horizontal phase speed change was small. These variations of the wave parameters, including the horizontal group velocity, amplitude, and its vertical wavenumber, are listed in Table 1.

Another very informative view of this event is demonstrated using keograms, which show time evolutions of data along the north–south and east–west axes of the image. The time series of the north–south slice across the center point of the AMTM images and the east–west counterpart are shown in Figure 4. The figure clearly indicates that the small-scale wave started appearing in the AMTM picture frame as early as ~ UT 03:25, from the southeast corner and traveling toward northwest. As the figure shows, the meridional component of the wave velocity slowed down considerably near UT 03:50 and became almost zero or "blocked" right before UT 04:00, along with the wave's zonal velocity component, showing a transition from traveling wave to a quasi-stationary wave. The wave went back to the traveling mode near UT 05:00 but appeared to be "reflected" toward southeast, opposite to its initial direction. This unique wave event ended around UT 05:30, when the wave almost fully dissipated. This wave "blocking and reflecting" event forms a characteristic "bullseye" feature in the keograms.

Utilizing the Gaussian-weighted fitting technique for AMTM temperature measurements (Zhao et al., 2005), the peak of the OH layer during the night of the event is estimated to be staying near 87 km throughout the night. At each time point, the lidar temperature is height-weighted using a 9-km FWHM Gaussian profile centered at assumed central heights between 82 and 92 km (in 0.1 km step). For altitudes below 90 km,

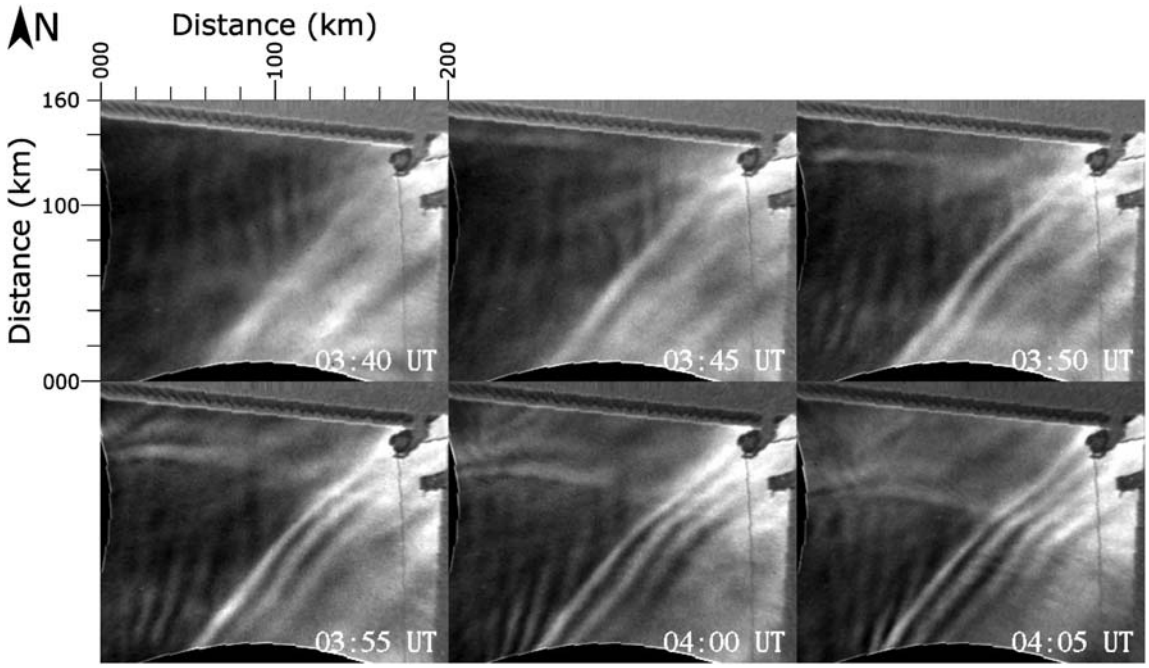

Figure 1. The AMTM-measured OH nightglow intensity variations at USU throughout the course of the wave "blocking" event captured on the night of 11 September 2016, between UT 03:40 and UT 04:05 every 5 min.

the Gaussian profile was truncated at altitudes where the lidar temperature errors increase due to the lower sodium density (lower signal level) at the edge of the sodium layer. The height-weighted lidar temperatures at different assumed central heights were then compared with the AMTM temperature values at the

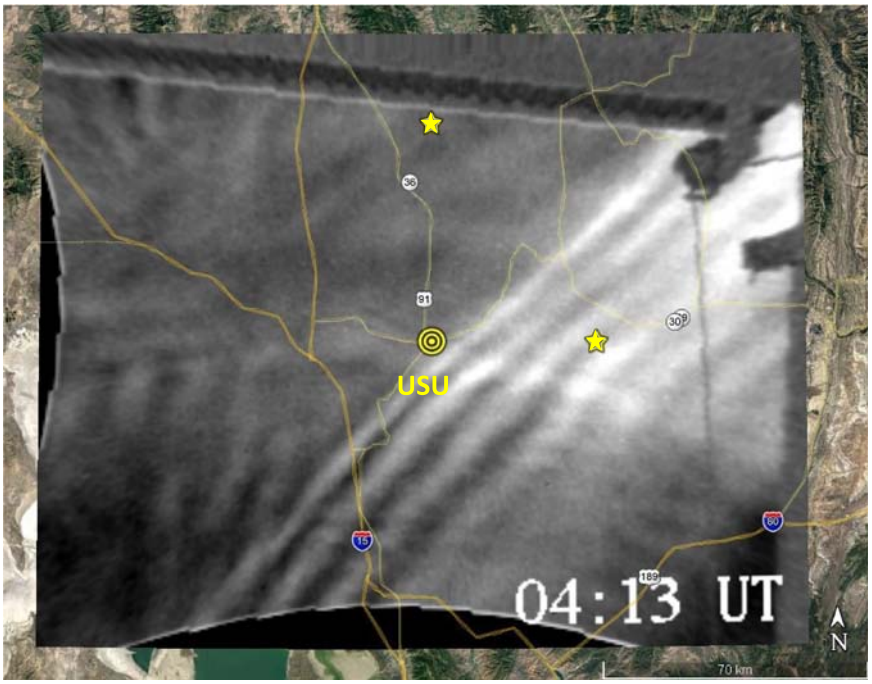

Figure 2. The OH nightglow intensity horizontal variation at UT 04:13 projected on top of the terrain map of northern Utah, when the wave became stationary. The orange stars mark the locations of two USU Na lidar beams at 87-km altitude, north-pointing beam (30° off zenith) and east-pointing beam (20° off zenith). The yellow dot in the center marks the USU location.

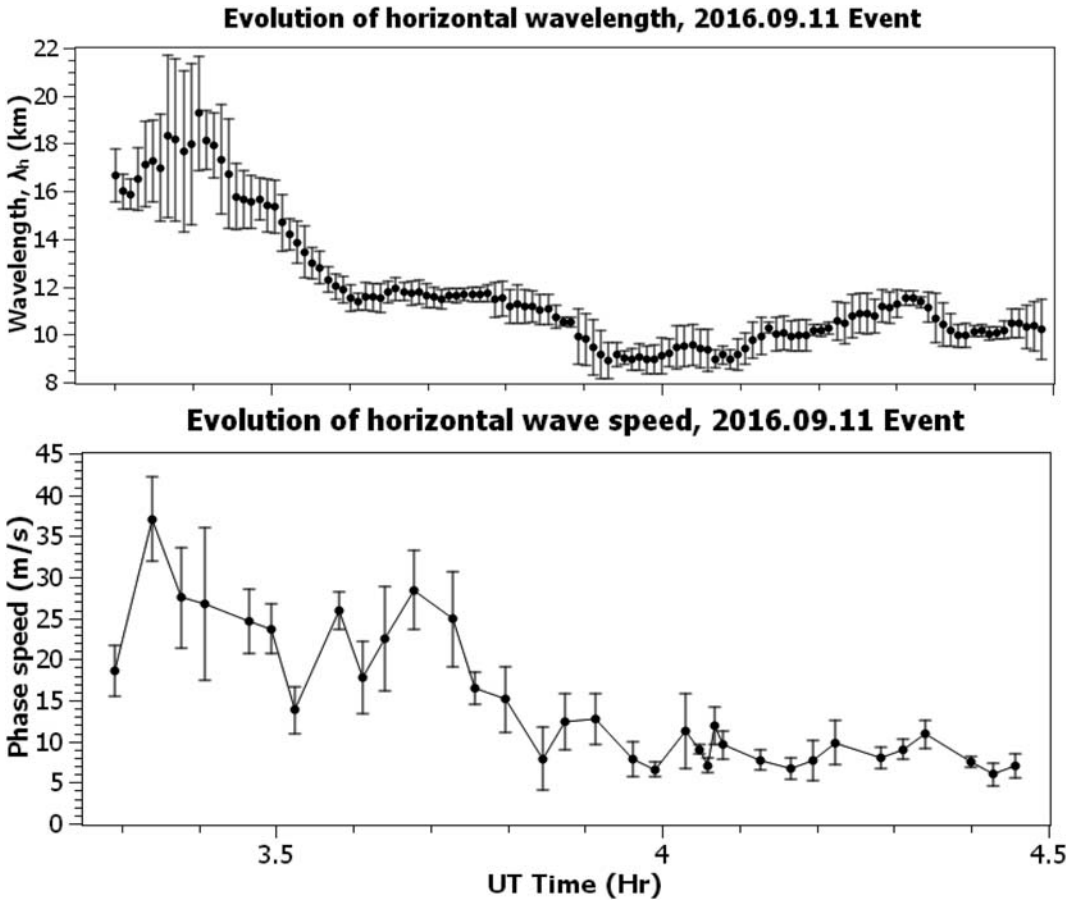

Figure 3. The time variations of the horizontal wavelength (top) and horizontal phase speed (bottom) of the "blocked" wave during the wave "blocking" event. The number of data point of the horizontal phase speed is less than those of the horizontal wavelength, because more frames of AMTM measurements are needed for its calculation.

corresponding time. The assumed altitude with the minimum difference between the weighted lidar temperature and AMTM temperature was selected as the OH peak height. The temperature horizontal structure at UT 04:10 along the wave propagation direction through the center point of AMTM are shown in Figure 5. The peak-to-peak value of the wave front reached ~5 K, when the wave became quasi-stationary at UT 04:05. As new crests are appearing, the trailing wave amplitude is decreasing, down to less than 2 K, similar to a mesospheric bore event (Dewan & Picard, 1998; Smith et al., 2005; Yue et al., 2009), except the changing of horizontal wavelength and the phase speed of the wave structure.

At the same time, the USU Na lidar observations provide the background atmosphere condition for this event. The lidar temperature measurements indicate the existence of a temperature inversion structure within the OH layer altitude range between UT 03:00 and UT 06:00 (see Figure 6) in both of the lidar

Table 1
Measured Wave and Background Parameters From AMTM, Lidar

Time (UT)	Temperature amplitude (K)	U_h (ms^{-1})		V_{ph} (ms^{-1})			V_g (ms^{-1})		k_h (km^{-1})	N^2 (s^{-2})	m^2 (km^{-2})	T (min.)
03:35	1	−37.06	19	±	5	13	±	7	0.24	.00064	1.38E-07	18.74
03:45	1	−43.28	19	±	5	8	±	4	0.36	.00053	1.01E-07	16.61
03:55	2	−42.96	9	±	3	7	±	3	0.38	.00053	1.77E-08	27.28
04:05	3	−51.28	9	±	2	6	±	4	0.52	.00043	8.31E-09	24.10n

Note. Headwind U_h, Brunt-Väisälä frequency squared N^2, and vertical wavenumber squared m^2 are each averages over 85–95 km altitude, our best estimate of the height of the OH layer, based on Na lidar data. Temperature amplitudes are based on horizontal AMTM temperature profiles.

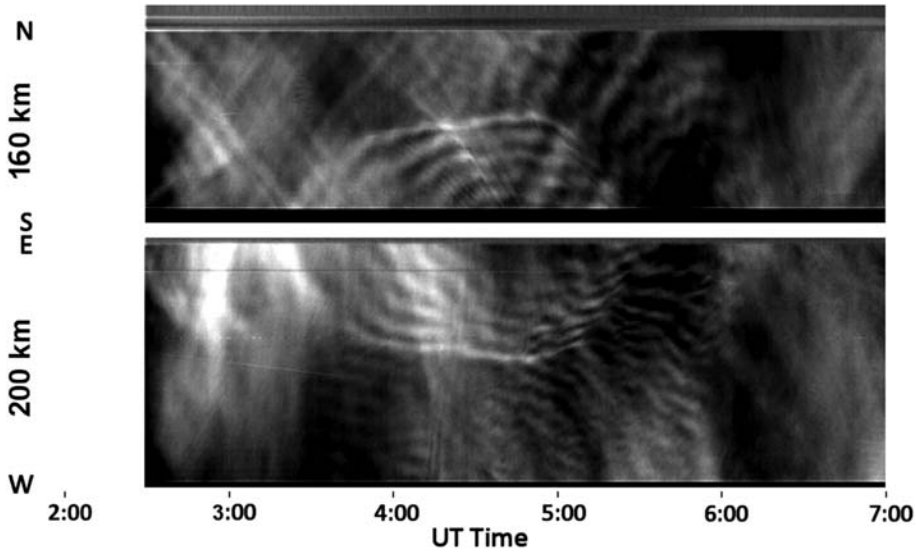

Figure 4. The USU AMTM keograms for the night of 11 September 2016. The north–south slice through the center point of AMTM field of view (top), and the west–east slice (bottom).

channels. Since the wave never reached the lidar north-pointing beam, the fact that this inversion layer appears in both lidar beams' temperature measurements indicates it is independent to this wave event. The inversion layer does appear to be interrupted at the time of wave "blocking" around UT 04:00 in the east channel, however. The mechanism of this inversion layer is not clear, but numerical studies suggest this temperature inversion layer could be related to the large tidal wave modulations of GW breaking (Liu et al., 2000; Liu & Hagan, 1998). Nevertheless, it facilitates the formation of stable layers (of high static stability) near and below the OH peak altitude. Intriguingly, the temperature inversion layer is one of the critical conditions for mesospheric bore propagation and constantly observed during the bore events (Smith et al., 2003; Yuan et al., 2014; Yue et al., 2009). Simultaneously, the USU Na lidar horizontal wind measurements provided the temporal variation of the horizontal wind projection in the initial small-scale wave propagating direction, which is illustrated in Figure 7. The lidar measurements show that the wave was experiencing a strong and increasing headwind throughout the event in the altitude range of the OH layer. Near UT 03:30, the headwind is ~50 m/s near 87 km. However, later on, the headwind increased to as much as ~65 m/s near UT 04:00. After UT 06:00, the wind changed its direction quickly, and, around UT 06:25, the projected horizontal wind became a tailwind, increasing to more than 20 m/s by UT 06:30. On the other hand, above 90 km, on the upper part of the OH layer, the projected horizontal wind remained as a tailwind for the wave throughout the night.

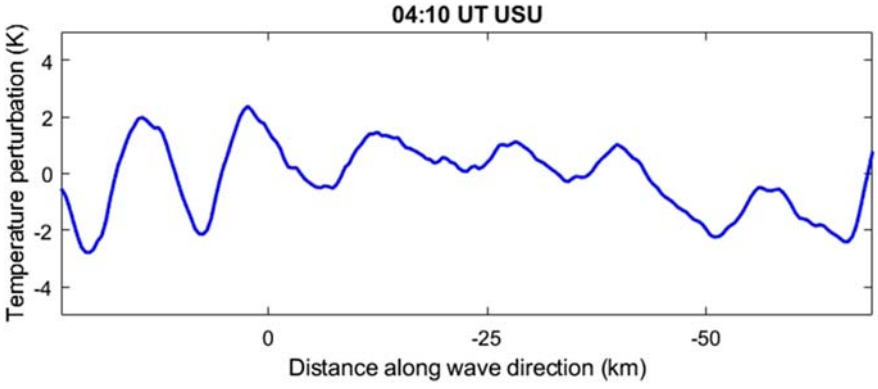

Figure 5. Horizontal temperature structure of the "blocked" wave at UT 04:10 along the wave propagation direction. The zero on the horizontal axis marks the center point of AMTM field of view.

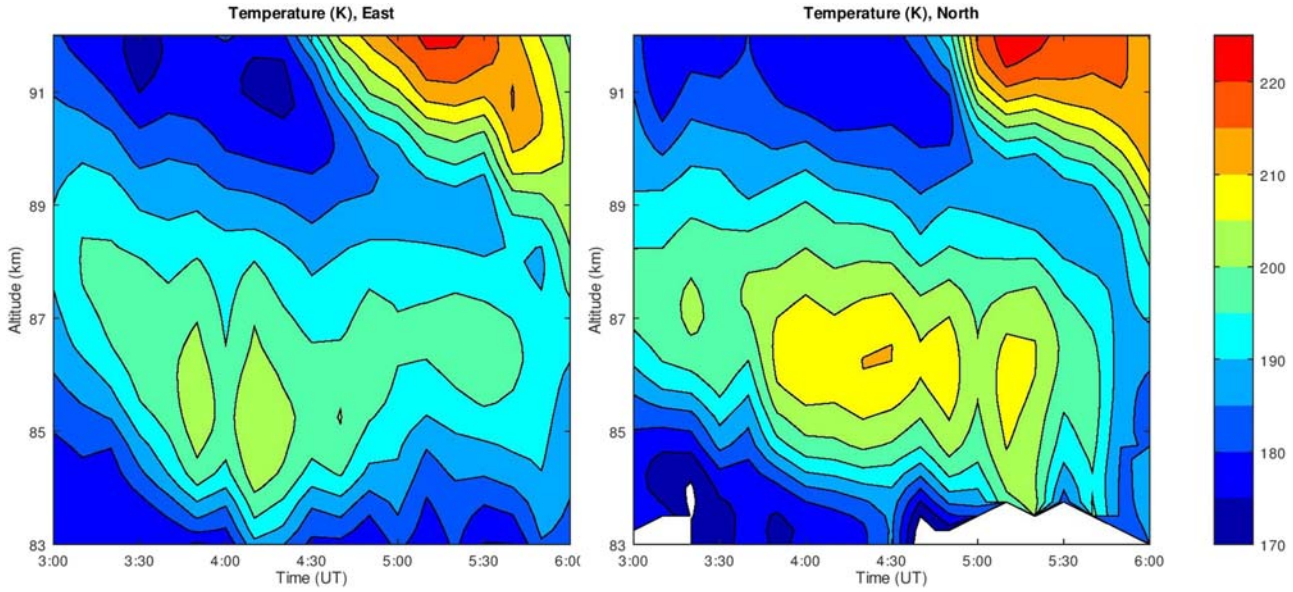

Figure 6. The USU Na lidar measured the time variations neutral temperature within the OH layer from east-pointing laser beam (left) and north-pointing laser beam (right) during the wave "blocking" event on the night of 11 September 2016.

GWs interact with their surrounding atmospheric background as they propagate through the wind fields. In addition to the aforementioned changes of intrinsic frequency, ω_i, and intrinsic phase velocity, c_i, the vertical wavenumber, m, and vertical wavelength in equation 1, λ_z, also vary with the projected horizontal wind through

$$m^2 = \frac{N^2}{(U_h - c)^2} - \frac{U_{zz}}{(U_h - c)} - k^2, \quad (1)$$

based on GW dispersion relation (Hooke, 1986), where N is the Brunt–Väisälä frequency. The Uzz and k are the second derivative of horizontal wind in wave direction and horizontal wavenumber, respectively. With the lidar-measured temperature and horizontal wind profiles, we calculated the variation of the vertical wavenumber square, m^2, of the "blocked" small-scale wave within the OH layer, as shown in Figure 8, along with the time variations of N^2. Because of the negative vertical temperature gradient in the upper part of the inversion layer, the atmosphere in top half of the OH layer became static unstable with negative N^2. The results indicate that the small-scale wave was initially propagating ($m^2 > 0$). Starting near UT 03:50, as the wave started getting "blocked" and "compressed" horizontally, its vertical wavenumber squared (m^2) decreased (indicating increasing vertical wavelength) and, eventually, became negative (evanescent) between 85 and 89 km. After UT 05:00, m^2 became positive (propagating) again near 87 km, and, throughout the event, no critical layer was formed within the OH layer (when vertical wavenumber goes to infinity). On top of the OH layer near and above 91 km, however, m^2 stayed positive throughout the night. Thus, this small-scale wave was likely ducted and trapped within the vicinity of the OH layer. This is quite different to the wave behavior reported in Yuan et al. (2014) at the same location observed on the night of 11 August 2011, when a small-scale wave packet (with similar propagating direction, horizontal scale and period) was "trapped" near 91 km within a temperature inversion layer but kept propagating horizontally (Figure 5 in Yuan et al., 2014) due to different horizontal background

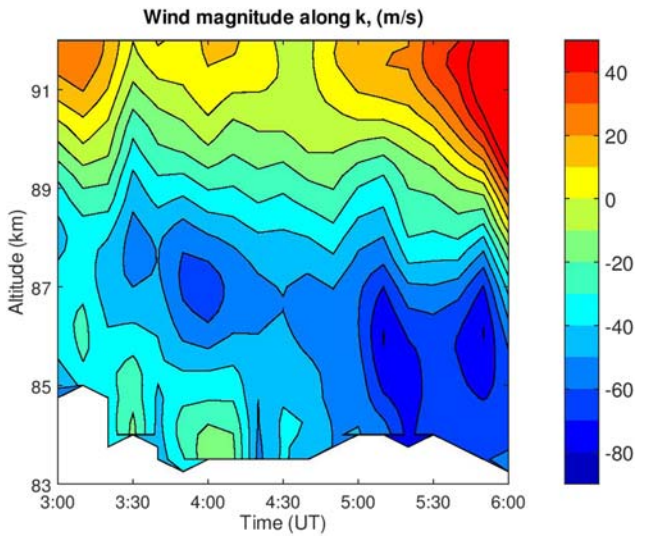

Figure 7. The USU Na lidar measured temporal variation of the horizontal wind projected onto the propagation direction of the "blocked" small-scale wave.

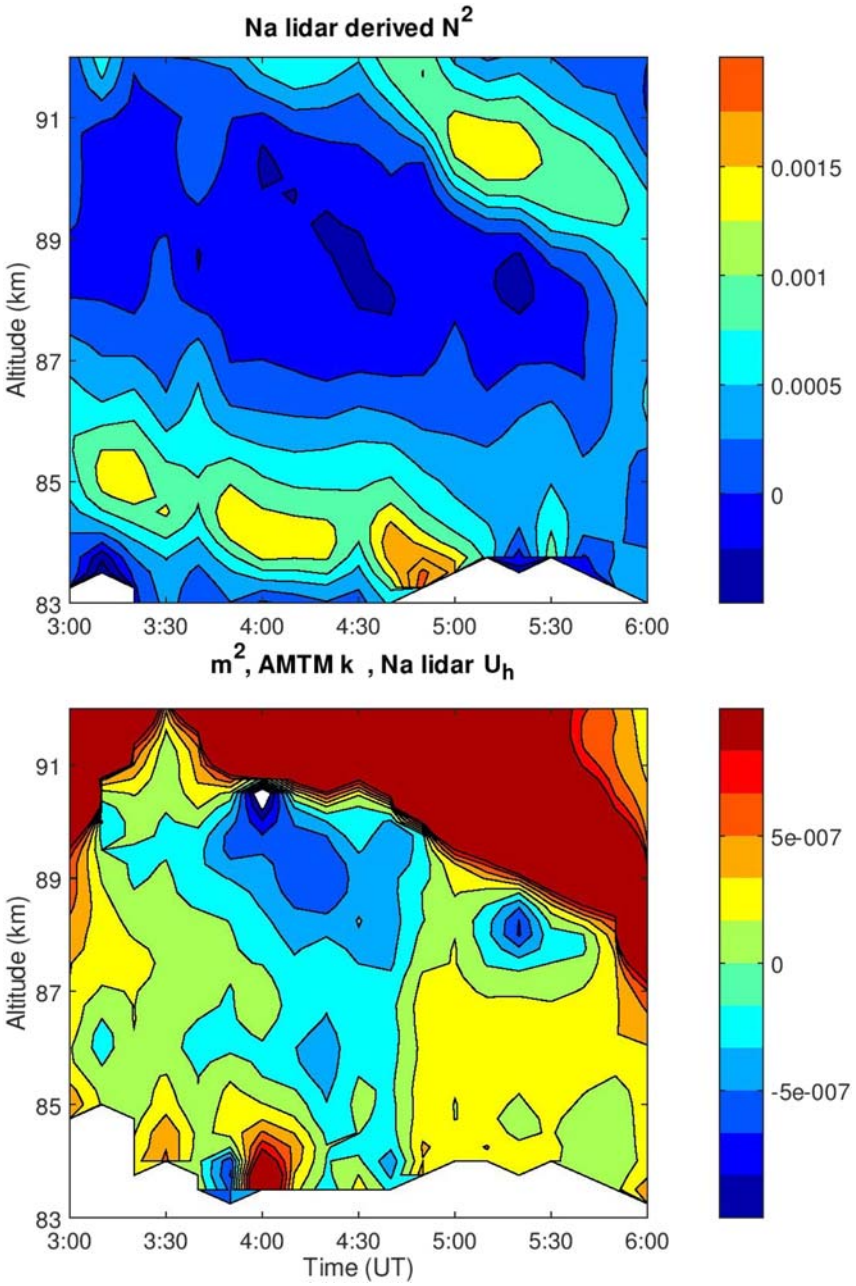

Figure 8. The calculated temporal variations of the Brunt-Väisälä frequency square (top) and the vertical wavenumber square (bottom) of the "blocked" small-scale wave, based on the AMTM and the Na lidar observations.

wind direction. The simultaneous N^2 observations (see Figure 8) by the lidar show the atmosphere near the upper part of the OH layer, where the N^2 became negative near 89 km, could be statically unstable, implicating potential wave breaking and dissipation above the OH layer.

4. Discussion

While the acceleration of horizontal wind, $\frac{dU_h}{dt}$, can contribute to the change of the wave's observed frequency and period ($\omega = \omega_i + kU_h$, ω is local/observed frequency, ω_i is intrinsic frequency), the calculation based on the AMTM and lidar wind measurements that night suggest such contribution-induced change of the observed wave period is quite small (less than 1 min). On the other hand, this observed wave event

matches well with the wave "blocking" phenomenon described in the theoretical work by Basovich and Tsimring (1984). They predicted that, when a wave is moving into a region of wind field against its direction of propagation, it will slow, steepen, and come to a halt. The wave could also be even "reflected" when the background wind reaches the blocking level,

$$u_0 = \frac{\left(N^{2/3} - \omega_i^{2/3}\right)^{3/2}}{m}. \tag{2}$$

Our calculation shows that the blocking level for this small-scale wave is about −54 m/s, and it agrees well with the observed projected wind within the OH layer by the lidar. The values of N and m are calculated based on the lidar and AMTM observations and averaged between UT03:20 and UT 03:50 within the altitude range of 85–89 km. As soon as the projected wind value exceeded the blocking value, the wave horizontal speed relative to the ground dropped to its slowest value (~ 5 ± 1 m/s).

In the latest numerical simulation work by Heale and Snively (2015), variations of a small-scale GW's propagation in different inhomogeneous horizontal wind fields are investigated in detail. Based on the ray trace equation from Lighthill (1978), in a varying atmospheric background (in the absence of viscosity), we have

$$\frac{dk}{dt} = -k\frac{dU_h}{dx}. \tag{3}$$

Thus, if there is a strong headwind (negative U_h) and large horizontal wind gradient exists, the horizontal wave number will increase, causing decreasing horizontal wavelength. At the same time, the wave's group velocity in horizontal direction can be written as

$$C_{gx} = \frac{\partial\omega}{\partial k} = U_h + \frac{m^2}{N^2}(c - U_h)^3. \tag{4}$$

It shows the horizontal group velocity of the wave is a function of the background wind and horizontal wavenumber, and, thus, the group velocity is quite sensitive to the change in horizontal wind. Therefore, it can be clearly seen that an increasing headwind would decrease the horizontal group velocity of the wave, which is consistent with the AMTM observation discussed earlier, illustrating the changing of the whole GW packet horizontal propagation, along with its horizontal phase speed. In the case of time independent, horizontally varying background wind, by assuming m and ω are constant throughout the process (simplifying the calculation without losing much of the geophysical process), Heale and Snively (2015) were able to reproduce the wave "blocking" and "compression" when the wave propagates against the background flow with a negative horizontal gradient, as time increases (Figure 3b in Heale and Snively (2015)). This simulated wave variation is very similar to the wave "blocking" described in Basovich and Tsimring (1984), in which the wave packet ceases to propagate horizontally and is even reflected as the wave crest moved against the flow. The simulation also indicates the increasing vertical wavelength of the small-scale wave during the "blocking" process.

Such wave phenomenon described in the numerical simulation and theoretical works above is extremely similar to the lidar-AMTM-observed small-scale wave variation on the night of 11 September 2016. Thus, this horizontal wave gradient mechanism is very likely the exact dynamical process that leads to the observed variation of the wave horizontal propagation. As a large amplitude wave propagates across a local station, in addition to the significant temporal variations of winds and temperature observed by the station, it also induces large horizontal gradients of the temperature and wind above, when the crest or trough of a large-scale wave approaches the station. Both large-scale tidal wave and GW are frequently observed in the MLT and are very likely sources of the potentially large horizontal wind gradient that evolves over time during this event. Indeed, the lidar horizontal wind measurement shows considerable wind change during the course of the wave "blocking" event at USU station that could be induced by some large-scale wave, such as the semidiurnal tide that dominates the MLT above the middle latitudes.

The above analysis assumes that the effects of the wave on the environment are limited and approximately linear. Some models show that GWs may self-accelerate by modulating the background wind (e.g., Fritts et al., 2015). This is most likely to occur in waves with large amplitudes and intrinsic phase velocities, so

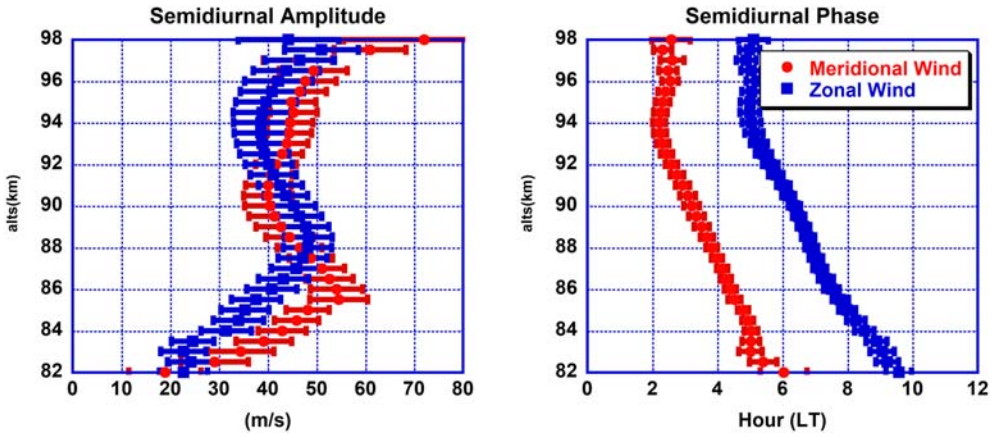

Figure 9. The Na lidar measured semidiurnal tidal amplitude and phase profiles of zonal and meridional wind during the 09–12 September period.

it is unlikely to be the case here. Further, wave dispersion associated with polychromatic wave packets has shown changing horizontal wave characteristics (e.g., Yuan et al., 2016), but the small-scale wave in this event is most likely constrained in its spectra and may even be subject to ducting implying discrete wave modes which are not subject to such dispersion.

With the full diurnal cycle capability, the USU Na lidar was running for almost 3 days continuously from UT 02:28 on 9 September to UT 01:42 on 12 September 2016. Migrating semidiurnal tide is found to be the dominant tidal wave in middle latitude of Northern America (Yuan et al., 2008, 2014). Based on this diurnal data set, Figure 9 illustrates the lidar observed semidiurnal amplitude and phase profiles during this campaign. These tidal wave parameters are derived based on the least-squared-fitting algorithm that includes all the tidal wave periods (24-, 12-, 8-, and 6-hr). The amplitude values of terdiurnal (8-hr) and quardiurnal (6-hr) tides are very small (both are less than 10 m/s) compared to that of the semidiurnal tide, while the diurnal tidal amplitude is less than half of the semidiurnal tidal amplitude. As the figure shows, both the zonal wind and meridional wind semidiurnal amplitudes have considerably large values (> 45 m/s) near the OH layer peak altitude, much larger than the reported climatological mean near this altitude (Yuan et al., 2008), and potentially generated a large horizontal wind gradient, as the tidal wave propagated horizontally across the lidar station. Thus, temporal modulations of the wind are readily identified in the data; however, the lidar provides only two points wind measurements (east and north) and, thus, cannot address

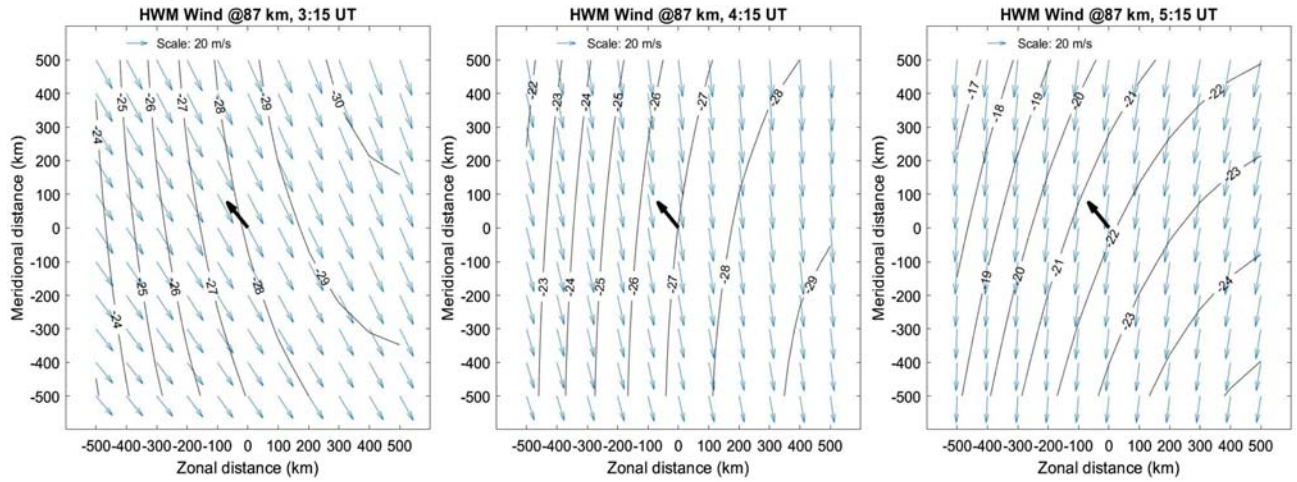

Figure 10. The horizontal wind data from HWM14 on the night of 11 September 2016 at UT 3:15 (left), UT 4:15 (middle), and UT 5:15 (right). The bold black arrows represent the wave propagation direction, and its origin represents the location of USU Na lidar station. The blue arrows represent the HWM14 horizontal wind, and the contour lines illustrate the horizontal wind projected onto the wave propagation direction.

the horizontal structure of the temperature and wind fields in MLT, not to mention the precise diagnosis of the large scale wave.

The AMTM can only measure the temporal variation of the horizontal temperature structure within the OH layer. Therefore, the existence of the large horizontal gradient of the headwind around the USU station is difficult to be confirmed by the observations of these two instruments. Nevertheless, the HWM14 (Drob et al., 2015) data on the same night have been investigated for the existence of such horizontal wind gradient near the lidar station (see Figure 10). In the wave propagation direction at 87 km, although the overall horizontal wind gradient is small, which is expected from an empirical model, the model results do show the existence of such gradient. The model also indicates a strong headwind relative to the wave (as much as ~28 m/s at UT 03:15) but with roughly half of the wind speed, compared with the lidar measurement in Figure 5. However, the model shows a decreasing headwind at this altitude, which is opposite to the lidar observations. As expected, the empirical model winds do not capture the variability present in reality; however, the similar mean directionality of the wind field as it varies over the course of the night is encouraging.

5. Summary

The USU AMTM captured a unique "blocked" wave event for the first time on the night of 11 September 2016, during a multiday collaborative campaign with the USU Na Temperature/Wind lidar. This event is characterized by a decreasing horizontal wavelength and horizontal phase speed. Theoretical and numerical simulation works have shown that a GW propagating through a large horizontal gradient in horizontal wind opposite to the wave propagating direction is expected to exhibit an increasing horizontal wavenumber and decreasing phase speed, extremely similar to the AMTM observation. The simultaneous USU Na lidar horizontal wind measurements indicate increasing headwind in the OH layer with respect to the "blocked" wave during the course of the event, which could be induced by some large-scale wave, such as tidal wave, that generated a large horizontal wind gradient at the nominal altitude of the OH layer when it was propagating across the USU station. The lidar-measured horizontal winds projected in the direction of wave motion reached and even slightly exceeded the blocking level as predicted by the theory, which coincides with the lowest measured wave speeds and shortest horizontal wavelengths. This suggests that the wave encounters a blocking level at this time due to a large negative horizontal wind gradient, possibly induced by tidal wave activity. Indeed, the lidar-measured semidiurnal tidal amplitudes of zonal and meridional winds during the campaign indicate large tidal wind amplitude, both exceeding 45 m/s at the altitude range of the OH layer and "blocking" altitudes.

This study has demonstrated highly complex variations of atmospheric GW horizontal propagation in the MLT, which are very sensitive to the relative direction of the horizontal wind and its horizontal gradient, including as they vary over time. Future work includes further detailed investigations of the dynamical mechanisms that may have created the conditions for blocking and refraction of this small-scale wave. Collaborative investigations including numerical modeling will also be essential to fully understand the geophysical processes that the observed wave event experienced.

Acknowledgments
This study was performed as part of a collaborative research program supported under the Consortium of Resonance and Rayleigh Lidars (CRRL), National Science Foundation grants AGS-1135882, AGS-1734333. The lidar and AMTM data of this study are available through "USU Na lidar and AMTM data structure for the "Blocking" wave project" (https:// doi.org/10.26078/217e-at74, Yuan, 2020). The authors also want to thank the Howard L. Blood Fellowship for its support of this project. The AMTM was developed under the Air Force DURIP grant F49620-02-1-0258 and operated through the NSF grant 1042227.

References

Basovich, A. Y., & Tsimring, L. S. (1984). Internal waves in a horizontally inhomogeneous flow. *Journal of Fluid Mechanics*, *142*, 233–249.

Becker, E., & Vadas, S. L. (2018). Secondary gravity waves in the winter mesosphere: Results from a high-resolution global circulation model. *Journal of Geophysical Research: Atmospheres*, *123*, 2605–2627. https://doi.org/10.1002/2017JD027460

Bossert, K., Fritts, D. C., Pautet, P. D., Williams, B. P., Taylor, M. J., Kaifler, B., et al. (2015). Momentum flux estimates accompanying multiscale gravity waves over Mount Cook, New Zealand, on 13 July 2014 during the DEEPWAVE campaign. *Journal of Geophysical Research: Atmospheres*, *120*, 9323–9337. https://doi.org/10.1002/2015JD023197

Bossert, K., Kruse, C. G., Heale, C. J., Fritts, D. C., Williams, B. P., Snively, J. B., et al. (2017). Secondary gravity wave generation over New Zealand during the DEEPWAVE campaign. *Journal of Geophysical Research: Atmospheres*, *122*, 7834–7850. https://doi.org/10.1002/2016JD026079

Cai, X., Yuan, T., Zhao, Y., Pautet, P.-D., Taylor, M. J., & Pendleton, W. R. Jr. (2014). A coordinated investigation of the gravity wave breaking and the associated dynamical instability by a Na lidar and an Advanced Mesosphere Temperature Mapper over Logan, UT (41.7N, 111.8W). *Journal of Geophysical Research: Space Physics*, *119*, 6852–6864. https://doi.org/10.1002/2014JA020131

Dewan, E., & Picard, R. (1998). Mesospheric bores. *Journal of Geophysical Research*, *103*(D6), 6295–6305.

Drob, D. P., Emmert, J. T., Meriwether, J. W., Makela, J. J., Doornbos, E., Conde, M., et al. (2015). An update to the Horizontal Wind Model (HWM): The quiet time thermosphere. *Earth and Space Science*, *2*, 301–319. https://doi.org/10.1002/2014EA000089

Fritts, D., & Alexander, M. J. (2003). Gravity wave dynamics and effects in the middle atmosphere. *Reviews of Geophysics*, *41*(1), 1003. https://doi.org/10.1029/2001RG000106

Fritts, D. C., Isler, J. R., Hecht, J. H., Walterscheid, R. L., & Andreassen, O. (1997). Wave breaking signatures in sodium densities and OH nightglow: 2. Simulation of wave and instability structures. *Journal of Geophysical Research*, *102*, 6669–6684.

Fritts, D. C., Laughman, B., Lund, T. S., & Snively, J. B. (2015). Self-acceleration and instability of gravity wave packets: 1. Effects of temporal localization. *Journal of Geophysical Research: Atmospheres*, *120*, 8783–8803. https://doi.org/10.1002/2015JD023363

Fritts, D. C., & Lund, T. S. (2011). Gravity wave influences in the thermosphere and ionosphere: Observations and recent modeling. In M. Abdu & D. Pancheva (Eds.), *Aeronomy of the Earth's atmosphere and ionosphere*, *IAGA Special Sopron Book Series* (Vol. 2, pp. 109–130). Dordrecht: Springer.

Fritts, D. C., Pautet, P.-D., Bossert, K., Taylor, M. J., Williams, B. P., Limura, H., et al. (2014). Quantifying gravity wave momentum flues with mesosphere temperature mappers and correlative instrumentation. *Journal of Geophysical Research: Atmospheres*, *119*, 13,583–13,603. https://doi.org/10.1002/2014JD022150

Heale, C. J., & Snively, J. B. (2015). Gravity wave propagation through a vertically and horizontally inhomogeneous background wind. *Journal of Geophysical Research: Atmospheres*, *120*, 5931–5950. https://doi.org/10.1002/2015JD023505

Hecht, J. H., Walterscheid, R. L., Fritts, D. C., Isler, J. R., Senft, D. C., Gardner, C. S., & Franke, S. J. (1997). Wave breaking signatures in OH airglow and sodium densities and temperature: 1. Airglow imaging, Na lidar, and MF radar observations. *Journal of Geophysical Research*, *102*, 6655–6668.

Holton, J. R. (1983). The influence of gravity wave breaking on the general circulation of the middle atmosphere. *Journal of the Atmospheric Sciences*, *40*, 2497–2507.

Hooke, W. H. (1986). Gravity waves. In P. S. Ray (Ed.), *Mesoscale meteorology and forecasting*, (pp. 272–288). Boston, Mass: Am. Meteorol. Soc.

Krueger, D. A., She, C. Y., & Yuan, T. (2015). Retrieving mesopause temperature and line-of-sight wind from full-diurnal-cycle Na lidar observations. *Applied Optics*, *54*(32), 9469–9489. https://doi.org/10.1364/AO.54.009469

Li, T., She, C. Y., Williams, B. P., Yuan, T., Collins, R. L., Kieffaber, L. M., & Peterson, A. W. (2005). Concurrent OH imager and sodium temperature/wind lidar observation of localized ripples over northern Colorado. *Journal of Geophysical Research*, *110*, D13110. https://doi.org/10.1029/2004JD004885

Lighthill, J. (1978). *Waves in fluids*. Cambridge: Cambridge University Press.

Liu, H., & Vadas, S. L. (2013). Large-scale ionospheric disturbances due to the dissipation of convectively-generated gravity waves over Brazil. *Journal of Geophysical Research: Atmospheres*, *118*, 2419–2427. https://doi.org/10.1002/jgra.50244

Liu, H.-L., & Hagan, M. E. (1998). Local heating/cooling of the mesosphere due to gravity wave and tidal coupling. *Geophysical Research Letters*, *25*, 2941–2944.

Liu, H.-L., Hagan, M. E., & Roble, R. G. (2000). Local mean state changes due to gravity wave breaking modulated by the diurnal tide. *Journal of Geophysical Research*, *105*, 12,381–12,396.

Lu, X., Chen, C., Huang, W., Smith, J. A., Chu, X., Yuan, T., et al. (2015). A coordinated study of 1-h mesoscale gravity waves propagating from Logan to Boulder with CRRL Na Doppler Lidars and Temperature Mapper. *Journal of Geophysical Research: Atmospheres*, *120*. https://doi.org/10.1002/2015JD023604

Pautet, P.-D., Taylor, M. J., Pendleton, W. R., Zhao, Y., Yuan, T., Esplin, R., & McLain, D. (2014). Advanced mesospheric temperature mapper for high-latitude airglow studies. *Applied Optics*, *53*(26), 5934–5943. https://doi.org/10.1364/AO.53.005934

Smith, S. M., Friedman, J., Raizada, S., Tepley, C., Baumgardner, J., & Mendillo, M. (2005). Evidence of mesospheric bore formation from a breaking gravity wave event: Simultaneous imaging and lidar measurements. *Journal of Atmospheric and Solar - Terrestrial Physics*, *67*(4), 345–356.

Smith, S. M., Taylor, M. J., Swenson, G. R., She, C.-Y., Hocking, W., Baumgardner, J., & Mendillo, M. (2003). A multidiagnostic investigation of the mesospheric bore phenomenon. *Journal of Geophysical Research*, *108*(A2), 1083. https://doi.org/10.1029/2002JA009500

Snively, J. B., & Pasko, V. P. (2008). Excitation of ducted gravity waves in the lower thermosphere by tropospheric sources. *Journal of Geophysical Research*, *113*, A06303. https://doi.org/10.1029/2007JA012693

Vadas, S. L., Fritts, D. C., & Alexander, M. J. (2003). Mechanism for the generation of secondary waves in wave breaking regions. *Journal of the Atmospheric Sciences*, *60*, 194–214. https://doi.org/10.1175/1520-0469(2003)060<0194:MFTGOS>2.0.CO;2

Yuan, T. (2020). USU Na lidar and AMTM data structure for the "Blocking" wave project, https://doi.org/10.26078/217e-at74

Yuan, T., Heale, C. J., Snively, J. B., Cai, X., Pautet, P.-D., Fish, C., et al. (2016). Evidence of dispersion and refraction of a spectrally broad gravity wave packet in the mesopause region observed by the Na lidar and Mesospheric Temperature Mapper above Logan, Utah. *Journal of Geophysical Research: Atmospheres*, *121*, 579–594. https://doi.org/10.1002/2015JD023685

Yuan, T., Pautet, P.-D., Zhao, Y., Cai, X., Criddle, N. R., Taylor, M. J., & Pendleton, W. R. Jr. (2014). Coordinated investigation of mid-latitude upper mesospheric temperature inversion layers and the associated gravity wave forcing by Na lidar and Advanced Mesospheric Temperature Mapper in Logan, Utah. *Journal of Geophysical Research: Atmospheres*, *119*, 3756–3769. https://doi.org/10.1002/2013JD020586

Yuan, T., Schmidt, H., She, C. Y., Krueger, D. A., & Reising, S. (2008). Seasonal variations of semidiurnal tidal perturbations in mesopause region temperature and zonal and meridional winds above Fort Collins, Colorado (40.6°N, 105.1°W). *Journal of Geophysical Research*, *113*, D20103. https://doi.org/10.1029/2007JD009687

Yue, J., She, C.-Y., Nakamura, T., Harrell, S., & Yuan, T. (2009). Mesospheric bore formation from large-scale gravity wave perturbations observed by collocated all-sky OH imager and sodium lidar. *Journal of Atmospheric and Solar—Terrestrial Physics*, *72*, 7–18.

Zhao, Y., Taylor, M. J., & Chu, X. (2005). Comparison of simultaneous Na lidar and mesospheric nightglow temperature measurements and the effects of tides on the emission layer heights. *Journal of Geophysical Research*, *110*, D09S07. https://doi.org/10.1029/2004JD005115